

## Application of Gaussian Error Propagation Principles for Theoretical Assessment of Model Uncertainty in Simulated Soil Processes Caused by Thermal and Hydraulic Parameters

NICOLE MÖLDERS, MIHAILO JANKOV, AND GERHARD KRAMM

*Geophysical Institute, University of Alaska Fairbanks, Fairbanks, Alaska*

(Manuscript received 29 July 2004, in final form 31 May 2005)

### ABSTRACT

Statistical uncertainty in soil temperature and volumetric water content and related moisture and heat fluxes predicted by a state-of-the-art soil module [embedded in a numerical weather prediction (NWP) model] is analyzed by Gaussian error-propagation (GEP) principles. This kind of uncertainty results from the indispensable use of empirical soil parameters. Since for the same thermodynamic and hydrological surface forcing and mean empirical parameters a soil module always provides the same mean value and standard deviation, uncertainty is first theoretically analyzed using artificial data for a wide range of soil conditions. Second, NWP results obtained for Alaska during a July episode are elucidated in relation to the authors' theoretical findings.

It is shown that uncertainty in predicted soil temperature and volumetric water content is of minor importance except during phase transition. Then the freeze–thaw term dominates and leads to soil temperature and moisture uncertainties of more than 15.8 K and  $0.212 \text{ m}^3 \text{ m}^{-3}$  in mineral soils. Heat-flux uncertainty is of the same order of magnitude as typical errors in soil-heat-flux measurements.

Uncertainty in the pore-size distribution index dominates uncertainty for all state variables and soil fluxes under most conditions. Uncertainties in hydraulic parameters (saturated hydraulic conductivity, pore-size distribution index, porosity, saturated water potential) affect soil-temperature uncertainty more than those in thermal parameters (density and specific heat capacity of dry soil material). Based on a thermal conductivity approach alternatively used, it is demonstrated that GEP principles are indispensable for evaluating parameterized soil-transfer processes.

Generally, statistical uncertainty decreases with depth. Close beneath the surface, the uncertainty in predicted soil temperature, volumetric water content, and soil-moisture and heat fluxes undergoes a diurnal cycle.

### 1. Introduction

All state-of-the-art numerical weather prediction models (NWPMs) and general circulation models (GCMs) use soil models embedded in so-called land surface models (LSMs) to predict the lower boundary conditions (thermodynamic and hydrological surface forcing), that is, temperature and specific humidity and fluxes of water vapor and sensible heat at the soil–atmosphere interface. These soil models have been developed based on the best knowledge of the scientific

community, and great efforts have been made to evaluate and improve them (e.g., Yang et al. 1995; Shao and Henderson-Sellers 1996; Lohmann et al. 1998; Mölders et al. 2003a). However, incomplete knowledge of initial conditions and soil type and heterogeneity may generally reduce the predictability of the soil state, fluxes of heat, water vapor, and water, and phase-transition processes within the soil and at the soil–atmosphere interface. The same is true when imperfect parameterizations for subgrid-scale processes, surface runoff, and cloud microphysical processes lead to an erroneous thermodynamic and hydrological surface forcing. Since NWPMs and GCMs are deterministic in nature, we must recognize that these shortcomings are systematic (or procedural) errors. Such errors, of course, can cause unacceptably great uncertainty in predicted results. Un-

---

*Corresponding author address:* Nicole Mölders, Geophysical Institute, University of Alaska Fairbanks, 903 Koyukuk Drive, P.O. Box 757320, Fairbanks, AK 99775-7320.  
E-mail: molders@gi.alaska.edu

fortunately, this uncertainty cannot be evaluated using statistical methods because procedural errors must generally be removed or, at least, minimized before statistical methods can be employed (e.g., Kreyszig 1970).

Much work has focused on identifying such procedural errors in the thermodynamic and hydrological surface forcing and evaluating the uncertainty they cause:

- (i) Uncertainty in the quantities at the surface that results from initializing soil-moisture and temperature distributions has already been investigated for various stand-alone versions of LSMs (e.g., Gao et al. 1996), NWPMs (e.g., Douville and Chauvin 2000), and GCMs (e.g., Wang and Kumar 1998). Adjoint models and data-assimilation techniques also have been applied for minimizing errors in initial soil conditions (e.g., van den Hurk et al. 1997; Callies et al. 1998; Reichle et al. 2001).
- (ii) Various sensitivity studies were performed to detect error sources related to presumptions and/or parameterization concepts (e.g., Robock et al. 1995; Cuenca et al. 1996; Shao and Irannejad 1999). The force-restore method, for instance, as it works with two or three reservoirs, has only limited ability to resolve soil horizons (Montaldo and Albertson 2001) and to simulate the vertical distributions of soil processes like the diurnal variation of the freezing line.
- (iii) Uncertainties related to parameterization of sub-grid-scale processes, surface runoff, and cloud microphysical processes including formation of precipitation, precipitation interception on different vegetation, and contribution of precipitation to thermodynamic and hydrological surface forcing have been evaluated by various authors (e.g., Avissar and Pielke 1989; Calder et al. 1995; Mölders et al. 1996, 1997; Niu and Yang 2004). Ideally, soil characteristics are mapped as continuous distributions to capture the gradients and mixtures in soil within a grid cell. Soils, however, are usually heterogeneous in space; consequently attributing a single soil type to an area of several square kilometers as is done in NWPM soil models can be ambiguous, and may surely be a source of errors. Using a wrong soil type, for instance, causes errors of more than 0.5 K and 0.5 g kg<sup>-1</sup> for near-surface air temperatures and humidity even in a 24-h simulation (Mölders 2001). It is well known that the variability in some soil parameters (e.g., hydraulic conductivity) is sometimes greater within the same soil type than across soil types. Observations show that heterogeneity within the

same soil may cause differences in evapotranspiration and recharge of 112 (14%) and 137 mm (4%) in 2050 days (Mölders et al. 2003b).

- (iv) Another kind of systematic error is related to the application of NWPMs themselves. Since the forecast range of such models is generally restricted to a week or so, predictions that violate this limitation of integration time can cause such great uncertainty that the results become worthless. This kind of uncertainty is well known and therefore not further discussed here.
- (v) Results from the Project for Intercomparison of Land Surface Parameterization Schemes (PILPS) showed that LSMs strongly differ in accuracy because of, among other things, the choice of empirical parameters required in parameterizations (e.g., Shao and Henderson-Sellers 1996; Slater et al. 1998). Usually, a mean value for a soil property derived from laboratory or/and field studies is attributed to a grid element (ignoring any kind of uncertainty). Consequently, predicted heat and matter fluxes and temperature and moisture distributions can vary over wide ranges depending on the choice of such empirical parameters, customarily considered as fixed during a simulation. If, for instance, distributions of prescribed coverage of land-use and soil types differ by about 5%, daily averages of the soil-moisture fraction alter by 0.19, a 29% change with respect to the reference case, and surface temperature by 2.3 K (Mölders et al. 1997). To assess whether slightly different parameters will result in significant perturbations of the model result, many simulations are required wherein (in the sense of parameter variation) only one parameter is altered at a time. Such parameter-variation studies are subject to so-called parameter interaction; that is, parameter choice affects other simulated quantities indirectly. Parameter effects or parameterization deficits that accidentally cancel each other out can remain overlooked (Henderson-Sellers 1993). To minimize parameter interaction these methods must be driven by either observation or reanalysis.

The inevitable use of empirical parameters in parameterizations for describing transfer processes leads to another source of uncertainty. Empirical parameters are generally burdened with “errors” arising from natural (random) variability as expressed by the variance or standard deviation. These standard deviations can be of the same order of magnitude as the parameters themselves (e.g., Clapp and Hornberger 1978; Cosby et al. 1984). Consequently, any quantity predicted with these

parameters is “error” burdened. Such uncertainty may even reduce the trust in short-term NWP and, in particular, the gain of credible information for agricultural use. In the case of climate simulations, this uncertainty may be a great burden in climate impact assessment. These errors are of random kind and, hence, can be evaluated with statistical methods.

To systematically investigate this statistical uncertainty that accompanies the predicted distributions of volumetric water content, soil temperature, and moisture and heat fluxes because of empirical soil parameters, we introduce Gaussian error-propagation (GEP) principles. The aim is to identify critical parameters (to prioritize which quantities to measure with higher accuracy), to point out parameterizations that cause high uncertainty due to their parameter dependency and the inherent statistical uncertainty, and to find possibilities for soil-modeling improvements. Since in a mathematical sense an equation to predict a flux/state variable and calculate the standard deviation is unambiguous, it will always provide the same flux/state variable and standard deviation for the same set of state variables and empirical parameters. Therefore, the statistical uncertainty of predicted soil conditions is first analyzed using artificial data for the typical range of thermodynamic and hydrological surface forcing. Doing so permits discussion of the spectrum from soil frost to relatively warm soil, and from dry to wet soil conditions. Second, to provide an example we assess the meaning of the theoretical findings for modeling by quantifying the model uncertainty throughout an NWP for Alaska during a summer episode.

## 2. Description of the NWP model

### a. Model setup

The fifth-generation Pennsylvania State University–National Center for Atmospheric Research (NCAR) Mesoscale Model (MM5) is the NWPM used in this study. As MM5 has evolved over the last decade and has been thoroughly documented and widely used (e.g., Dudhia 1993; Chen and Dudhia 2001), the model setup is only briefly described.

Cloud microphysical processes are predicted by Reisner et al.’s (1998) mixed-phase scheme that distinguishes between cloud water, rainwater, ice, snow, and graupel. As the horizontal resolution (45 km) considerably exceeds the typical horizontal extension of cumulus clouds, a cumulus parameterization is inevitable (e.g., Raymond and Emanuel 1993), for which we use Grell et al.’s (1991) cumulus scheme. Additionally, Grell et al.’s (1994) simple radiation scheme is considered. The turbulent transfer processes are parameter-

ized according to Hong and Pan (1996). The hydrothermodynamic soil–vegetation scheme (HTSVS) serves to determine the lower boundary conditions of MM5, that is, temperature and specific humidity and exchange of momentum, heat, and moisture at the earth–atmosphere interface. HTSVS consists of a multilayer soil model, a single-layer canopy model (Kramm et al. 1994, 1996; Mölders et al. 2003a), and a multilayer snow model (Mölders and Walsh 2004). Long-term (2050 days) evaluations demonstrated that HTSVS simulates accumulated groundwater recharge, evapotranspiration, and soil temperatures within 15% and on average about 1–2-K accuracy without calibration (Mölders et al. 2003a,b).

### b. Soil model

The soil model is based on the principles of the linear thermodynamics of irreversible processes (e.g., de Groot 1951). It deals with soil freezing/thawing and (vertical) heat- and water-transfer processes (including the Richards equation) quantified by the balance equations for heat and moisture (e.g., Philip and de Vries 1957; de Vries 1958; Kramm et al. 1994, 1996; Mölders et al. 2003a),

$$C \frac{\partial T_S}{\partial t} = \frac{\partial}{\partial z_S} \left( \lambda \frac{\partial T_S}{\partial z_S} \right) + \frac{\partial}{\partial z_S} \left( L_v \rho_w D_{Tv} \frac{\partial T_S}{\partial z_S} \right) + \frac{\partial}{\partial z_S} \left( L_v \rho_w D_{\eta v} \frac{\partial \eta}{\partial z_S} \right) + L_f \rho_{\text{ice}} \frac{\partial \eta_{\text{ice}}}{\partial t}, \quad (1)$$

$$\frac{\partial \eta}{\partial t} = \frac{\partial}{\partial z_S} \left( D_{\eta v} \frac{\partial \eta}{\partial z_S} \right) + \frac{\partial}{\partial z_S} \left( D_{\eta l} \frac{\partial \eta}{\partial z_S} \right) + \frac{\partial}{\partial z_S} \left( D_{Tv} \frac{\partial T_S}{\partial z_S} \right) + \frac{\partial K_w}{\partial z_S} - \frac{\chi}{\rho_w} - \frac{\rho_{\text{ice}}}{\rho_w} \frac{\partial \eta_{\text{ice}}}{\partial t}. \quad (2)$$

Here,  $z_S$  is soil depth, and  $\chi$  represents water uptake per soil volume by roots;

$$D_{\eta v} = -\alpha D_w b \frac{\eta_s - \eta}{\eta} \frac{\rho_a}{\rho_w} \frac{g\psi}{R_d T_S}, \quad (3)$$

$$D_{Tv} = \alpha D_w (\eta_s - \eta) \frac{\rho_a}{\rho_w} \frac{L_v - g\psi}{R_d T_S^2}, \quad (4)$$

and

$$D_{\eta l} = -\frac{b k_s \psi_s}{\eta} \left( \frac{\eta}{\eta_s} \right)^{b+3} \quad (5)$$

are transfer coefficients for water vapor, heat, and water with  $\alpha$ ,  $D_w$ ,  $\eta_s$ ,  $b$ ,  $\psi_s$ ,  $k_s$ , and  $R_d$  being torsion factor, molecular diffusion coefficient of water vapor, porosity, pore-size distribution index, saturated water potential,

saturated hydraulic conductivity, and dry air gas constant, respectively. The variables  $T_s$ ,  $\eta$ , and  $\eta_{ice}$  are soil temperature, volumetric water, and ice content. Furthermore,

$$K_w = k_s W^{2b+3} \quad (6)$$

is hydraulic conductivity, where  $W = \eta/\eta_s$  is relative volumetric water content (e.g., Clapp and Hornberger 1978). Volumetric heat capacity of moist soil is given by (e.g., Mölders et al. 2003a)

$$\lambda = \begin{cases} 419 \exp\{-(2 + {}^{10}\log|\psi| + 2.7)\} & 2 + {}^{10}\log|\psi| < 5.1 \\ 0.172 & 2 + {}^{10}\log|\psi| \geq 5.1 \end{cases} \quad (8)$$

depends on water potential (e.g., Flerchinger and Saxton 1989)

$$\psi = \begin{cases} \psi_s W^{-b} & T_s > 273.15 \text{ K} \\ L_f \frac{T_s - 273.15}{g T_s} & T_s \leq 273.15 \text{ K} \end{cases} \quad (9)$$

where  $g$  is acceleration due to gravity. Below 273.15 K, mass-weighted thermal conductivity depending on volumetric water and ice content is calculated using Eq. (8) for the liquid and  $2.31 \text{ J (m s K)}^{-1}$  for the solid phase.

In Eq. (1), the first term on the right-hand side addresses soil-temperature changes by divergence of soil-heat fluxes. The second term denotes the divergence of soil-heat fluxes due to water vapor transfer, the third refers to the Dufour effect (i.e., a moisture gradient contributes to a soil-temperature change), and the last term gives changes due to freezing/thawing. The first two terms on the right-hand side of Eq. (2) give the changes in volumetric water content due to divergence of water vapor and water fluxes. The third term represents the Ludwig–Soret effect (i.e., a temperature gradient contributes to a volumetric water-content change), the fourth denotes changes due to hydraulic conductivity, the fifth is water uptake by roots, and the last describes freezing/thawing. The Dufour and Ludwig–Soret effects are usually considered cross phenomena in the thermodynamics of irreversible processes.

At temperatures below freezing, water and ice can coexist in soils. The maximum amount of supercooled water that may exist is given by (e.g., Flerchinger and Saxton 1989)

$$\eta_{\max} = \eta_s \left\{ \frac{L_f (T_s - 273.15)}{g \psi_s T_s} \right\}^{-1/b} \quad (10)$$

$$C = (1 - \eta_s) \rho_s c_s + \eta \rho_w c_w + \eta_{ice} \rho_{ice} c_{ice} + (\eta_s - \eta - \eta_{ice}) \rho_a c_p, \quad (7)$$

where  $\rho_s$ ,  $\rho_w$ , and  $\rho_{ice}$  are densities of dry soil material, water, and ice;  $c_s$ ,  $c_w$ , and  $c_{ice}$  are the corresponding specific heats. Moreover,  $\rho_a$  and  $c_p$  are the density of air and specific heat at constant pressure;  $L_v$  and  $L_f$  are the latent heats of vaporization and freezing.

In accord with McCumber and Pielke (1981), thermal conductivity,

As most state-of-the-art soil models (e.g., Sievers et al. 1987; Verseghy 1991; Viterbo and Beljaars 1995; Wetzel and Boone 1995; Yang et al. 1997; Slater et al. 1998; Viterbo et al. 1999; Chen and Dudhia 2001; War-rach et al. 2001) are based on variations or simplified versions of Eqs. (1)–(10), the following uncertainty analysis of their terms permits generalizing.

### c. Model domain

The model domain (Fig. 1) has  $39 \times 39$  points, a horizontal grid spacing of 45 km, and 23 vertical layers reaching to 100 hPa. There are five snow layers of equal thickness depending on snow depth. The uppermost

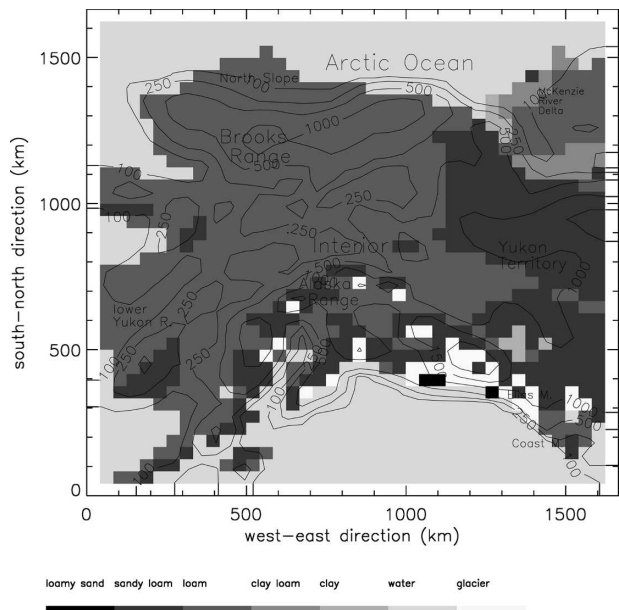


FIG. 1. Soil-type distribution and topography as used in the study.

soil layer ranges from the surface to the uppermost level within the soil at 0.1-m depth. Between that level and the lowest level at 2.95-m depth, there are four layers spaced by the same logarithmic increment so that central differences can be used in solving the coupled Eqs. (1) and (2) by a generalized Crank–Nicholson scheme. The time step is 135 s.

#### d. Synoptic situation

The episode covers 0000 UTC 20 July to 1200 UTC 23 July 2001. During this period, weather was driven by cyclonal activity within a large-scale trough over the North Pacific and Bering Sea. The long-wave disturbance propagated eastward and established a weak-gradient spacious trough over Alaska in the middle and toward the end of the episode. On the surface, Alaska remained on the outer edge of a well-developed eastward-moving cyclone located north of Siberia. This synoptic pattern was favorable for heavy thunderstorms over the Alaska and Brooks Ranges and the Interior. During the episode, low-elevation near-surface air and dewpoint temperatures ranged from 8° to 22°C and −1° to 16°C, respectively. Sunrise (sunset) is around 0300 (2100), 0400 (2330), and 0530 (0100) Alaska standard time (AST; UTC minus 9 h) in the eastern, central, and western parts of the domain. While the sun barely goes below the horizon in the north, sunrise (sunset) is around 0500 (2300) AST in the southern central part of the domain.

#### e. Initialization

Initial and boundary conditions are obtained from the National Centers for Environmental Prediction (NECP)–NCAR reanalysis project (NNRP). The vegetation fraction of each grid cell is a weighted combination of July and August monthly 5-yr-mean green vegetation cover (0.15° resolution) derived from Advanced Very High Resolution Radiometer (AVHRR) data (Gutman and Ignatov 1998). Soil texture, terrain elevation (Fig. 1), and land use are taken from the 1-km-resolution U.S. Department of Agriculture (USDA) State Soil Geographic Database (Miller and White 1998) and 10-min-resolution U.S. Geological Survey (USGS) terrain and vegetation data.

Initial total soil moisture and temperature are interpolated from NNRP data. Total moisture partitioning between liquid and solid phases follows Mölders and Walsh (2004). No assumptions about active layer depth are required as HTSVS works for both active layer and permafrost. Temperature, volumetric water, and ice content at the bottom of the soil model are constant throughout the simulation.

### 3. Method

#### a. Gaussian error propagation

The state quantities  $\eta(\eta_s, \psi_s, b, k_s)$  and  $T_s(\eta_s, k_s, b, \rho_s, c_s)$  and the related moisture  $W_s(\eta_s, \psi_s, b, k_s)$  and heat  $H_s(\eta_s, \psi_s, b, \rho_s, c_s)$  fluxes are “error” burdened by an amount  $\sigma_\phi$  resulting from the random variability of empirical parameters usually characterized by standard deviations. To determine model uncertainty caused by empirical soil parameters for  $\eta$ ,  $T_s$ ,  $W_s$ , and  $H_s$  at the surface and various depths, we consider GEP principles. In doing so, the equation to predict a quantity  $\phi$  (e.g.,  $\eta$ ) is derived for all empirical parameters  $\chi_i$  on which it depends (e.g.,  $\eta_s$ ,  $\psi_s$ ,  $b$ , and  $k_s$ ). The standard deviation (statistical uncertainty) of the predicted quantity can be calculated from these individual derivations ( $\partial\phi/\partial\chi_i$ ) and the standard deviations  $\sigma_{\chi_i}$  of the  $i$ th empirical parameters  $\chi_i$  by (e.g., Kreyszig 1970)

$$\sigma_\phi = \sqrt{\sum_{i=1}^n \left(\frac{\partial\phi}{\partial\chi_i}\right)^2 \sigma_{\chi_i}^2} = \sqrt{\sum_{i=1}^n \{\phi, \sigma_{\chi_i}\}^2}, \quad (11)$$

where  $n$  is the number of parameters,  $\sigma_{\chi_i}^2$  are the variances, and  $(\partial\phi/\partial\chi_i)\sigma_{\chi_i} := \{\phi, \sigma_{\chi_i}\}$  and  $\sigma_\phi$  are denoted contribution (term) and uncertainty, hereafter. The relative error is defined by  $\varepsilon_\phi = (\sigma_\phi/\phi)$ . Note that one standard deviation means that 68.27% of all values fall within  $\phi \pm \sigma_\phi$ .

Equation (11) assumes that 1) errors are normal distributed and 2) errors are independent between various model parameters, which is justified for these parameters. Standard deviations of  $\eta_s$ ,  $\psi_s$ ,  $b$ , and  $k_s$  are taken from Clapp and Hornberger (1978) and Cosby et al. (1984) for mineral soils. Standard deviations for organic soils and  $\rho_s$ , and  $c_s$  are collected from various sources (Table 1). To our best knowledge there are no studies on the sensitivity of the parameter variance at different temperature and moisture conditions. Therefore, as common practice in soil modeling, we assume these parameters and their variances as independent of the state variables.

#### b. Uncertainty analysis

According to Eq. (11), any set of mean parameters and their standard deviations always provide the same standard deviation of a predicted quantity for the same soil conditions. Therefore, equations for  $\eta$ ,  $T_s$ ,  $W_s$ , and  $H_s$  and the respective equations for standard deviation are applied for typical soil-forcing ranges. Fluxes and their standard deviations are calculated for soil temperatures and volumetric water content from −20° to 30°C and 0.001 to porosity, respectively. Soil-moisture

TABLE 1. Soil characteristics for soils considered in this study. Here,  $k_s$ ,  $\eta_s$ ,  $b$ ,  $\psi_s$ ,  $c_s$ , and  $\rho_s$  are the saturated hydraulic conductivity, porosity (saturated volumetric water content), pore-size distribution index, saturated water potential, as well as the specific heat capacity and density of the dry soil material. Parameters plus/minus their standard deviations for  $k_s$ ,  $\eta_s$ ,  $b$ , and  $\psi_s$  are from Cosby et al. (1984). Values in parentheses denote the relative error in %.

Soil type	$k_s$ $10^{-6}$ (m s $^{-1}$ )	$\eta_s$ (m $^3$ m $^{-3}$ )	$b$ -,-	$\psi_s$ (m)	$\rho_s$ (kg m $^{-3}$ )	$c_s$ [J (kg K) $^{-1}$ ]
Sand	46.8 $\pm$ 16.29 (34.81)	0.339 $\pm$ 0.073 (21.53)	2.79 $\pm$ 1.38 (49.46)	-0.069 $\pm$ 0.036 (52.17)	1580 $\pm$ 90 (5.70) <sup>a</sup>	930 $\pm$ 76 (8.17)
Loamy sand	14.19 $\pm$ 23.7 (167.02)	0.421 $\pm$ 0.072 (17.10)	4.26 $\pm$ 1.95 (45.77)	-0.0361 $\pm$ 0.0537 (149)	1610 $\pm$ 100(6.21) <sup>a</sup>	876 $\pm$ 69 (7.88)
Sandy loam	5.27 $\pm$ 1.52 (28.84)	0.474 $\pm$ 0.088 (1.69)	4.74 $\pm$ 1.40 (29.53)	-0.141 $\pm$ 0.0537 (38.09)	1520 $\pm$ 140(9.21) <sup>a</sup>	882 $\pm$ 34 (3.85)
Silt loam	2.83 $\pm$ 2.00 (70.67)	0.434 $\pm$ 0.054 (12.44)	5.33 $\pm$ 1.72 (32.27)	-0.759 $\pm$ 0.024 (3.16)	1400 $\pm$ 90 (6.43) <sup>a</sup>	907 $\pm$ 69 (7.61)
Loam	3.38 $\pm$ 1.67 (49.41)	0.439 $\pm$ 0.074 (16.86)	5.25 $\pm$ 1.66 (31.62)	-0.355 $\pm$ 0.0457 (12.87)	1350 $\pm$ 110 (8.15) <sup>a</sup>	896 $\pm$ 52 (5.80)
Sandy clay loam	4.487 $\pm$ 2.05 (45.69)	0.404 $\pm$ 0.048 (11.88)	6.77 $\pm$ 3.39 (50.07)	-0.135 $\pm$ 0.11 (81.48)	1520 $\pm$ 40 (2.63) <sup>a</sup>	776 $\pm$ 75 (9.66)
Silty clay loam	2.051 $\pm$ 1.75 (85.32)	0.464 $\pm$ 0.046 (9.91)	8.72 $\pm$ 4.33 (49.66)	-0.617 $\pm$ 0.038 (6.16)	1410 $\pm$ 60 (4.26)	936 $\pm$ 85 (9.08)
Clay loam	2.466 $\pm$ 1.83 (74.21)	0.465 $\pm$ 0.054 (11.61)	8.17 $\pm$ 3.74 (45.78)	-0.263 $\pm$ 0.055 (20.91)	1420 $\pm$ 80 (5.63) <sup>a</sup>	866 $\pm$ 72 (8.31)
Sandy clay	7.28 $\pm$ 1.50 (20.60)	0.406 $\pm$ 0.032 (7.88)	10.73 $\pm$ 1.54 (14.35)	-0.098 $\pm$ 0.0363 (37.04)	1570 $\pm$ 120 (7.64) <sup>a</sup>	783 $\pm$ 48 (6.13)
Silty clay	1.355 $\pm$ 1.45 (100.70)	0.468 $\pm$ 0.062 (13.25)	10.39 $\pm$ 4.27 (41.10)	-0.324 $\pm$ 0.069 (21.30)	1480 $\pm$ 110 (7.43) <sup>a</sup>	797 $\pm$ 52 (6.52)
Clay	0.9816 $\pm$ 1.705 (170.37)	0.468 $\pm$ 0.035 (7.48)	11.55 $\pm$ 3.93 (34.03)	-0.468 $\pm$ 0.039 (8.33)	1470 $\pm$ 140 (9.52) <sup>b</sup>	890 $\pm$ 23 (2.58)
Peat soil	1.736 $\pm$ 0.938 (54.03) <sup>c</sup>	0.923 $\pm$ 0.342 (37.05)	4.00 $\pm$ 1.75 (43.75)	-0.165 $\pm$ 0.31 (188)	106 $\pm$ 243 (229)	1920 $\pm$ 100 (5.21)
Moss soil	150 $\pm$ 400 (266.67) <sup>d</sup>	0.900 $\pm$ 0.040 (4.44)	1.00 $\pm$ 1.75 (175)	-0.120 $\pm$ 0.310 (258)	100 $\pm$ 100 (100)	10 000 $\pm$ 100 (1)
Lichen soil	3356.5 $\pm$ 200 (5.96) <sup>e</sup>	0.95 $\pm$ 0.060 (6.67)	0.50 $\pm$ 1.75 (350)	-0.085 $\pm$ 0.310 (365)	120 $\pm$ 30 (25.00)	8333 $\pm$ 100 (1.2)

<sup>a</sup> Grunwald et al. (2001).

<sup>b</sup> Calhoun et al. (2001).

<sup>c</sup> Schlotzhauer and Price (1999).

<sup>d</sup> Carey and Woo (1999).

<sup>e</sup> Laurén and Heiskanen (1997).

and temperature gradients are varied from  $-200$  to  $200 \text{ m}^3 \text{ m}^{-3} (\text{m}^{-1})$  and  $-200$  to  $200 \text{ K m}^{-1}$ .

To identify critical parameters we estimate the contributions of individual parameters to the uncertainty by analyzing the various terms  $\{\phi, \sigma_{\chi_i}\}$ . Ideally all terms  $\{\phi, \sigma_{\chi_i}\}$  are of the same order of magnitude for a good parameterization and parameter set. A parameter  $\chi_k$  will be identified as critical if  $\{\phi, \sigma_{\chi_k}\}$  exceeds all other terms  $\{\phi, \sigma_{\chi_i}\}_{i \neq k}$  by more than an order of magnitude. A parameterization (or parts of it) will be classified as critical if its dependent parameters lead to a huge standard deviation in this parameterization, but do not provide great uncertainty in another parameterization of the soil model.

As mentioned before, an MM5 simulation is performed for Alaska during a summer period to demonstrate the meaning of the theoretical results for NWP and to elucidate the limit of predictability. For these purposes, the uncertainty-analysis tool was implemented into MM5 to avoid improper data handling by a postprocessor. This supplementary module, of course, does not affect any simulation results. Since MM5 starts without clouds it takes a certain amount of time until clouds form in MM5, leading to excessive insolation during spinup (systematic errors). Thus, the discussion focuses on results after spinup. As common practice in NWPMs, we assume each MM5 grid cell to be homogeneously taken by one soil type at all depths. Note that if soil types varied horizontally and/or vertically within a grid cell, spatial derivations would have to be included in Eq. (11) and results may become scale dependent.

#### 4. Results

Typically, total moisture (water plus ice) increases with depth. In permafrost, temperatures are below  $0^\circ\text{C}$  for at least two consecutive years; total moisture is close to porosity. In the active layer, the frozen water fraction increases with depth. Desert soils are dry and hot; soils on desert plateaus dry but cold; and soils in the Tropics warm and wet. Moderately wet, near- $0^\circ\text{C}$  conditions correspond to midlatitude winters. Snowmelt and rain yield wet conditions at temperatures around and above  $0^\circ\text{C}$ , respectively.

Because of atmospheric forcing soil-temperature and moisture gradients are greater close beneath the surface than in deeper soil layers. Close to the surface,  $\eta$ ,  $T_s$ ,  $W_s$ , and  $H_s$  undergo a diurnal cycle. Rain and snowmelt (evapotranspiration) produce downward (upward) soil-moisture fluxes.

Soils with no clay but high sand fraction permit the lowest, and clay-containing soils the greatest, fraction of supercooled water (Fig. 2). At  $0^\circ\text{C}$ , the maximum

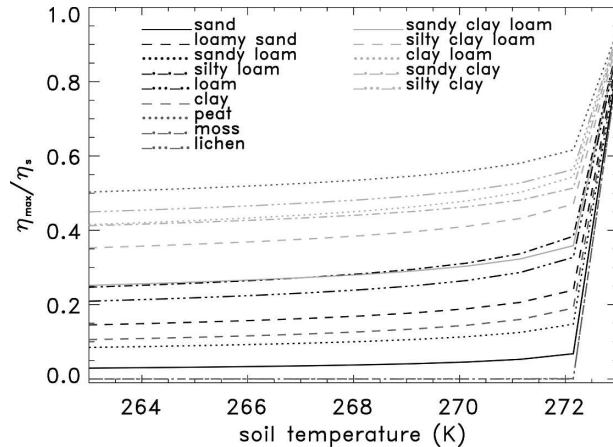


FIG. 2. Freezing characteristic curve showing the dependence of maximum relative supercooled water content  $\eta_{\max}/\eta_s$  on soil temperature for selected soils. Note that relative water content ranges between 0 and 1 and is dimensionless.

allowable supercooled water drops to 50% of porosity for all soils except for silty clay loam, sandy clay loam, silt clay, and clay that reach this condition at  $-3^\circ$ ,  $-2^\circ$ ,  $-4^\circ$ , and  $-11^\circ\text{C}$ , respectively. Supercooled water hardly exists in moss. At  $-11^\circ\text{C}$ , the maximum allowable supercooled water falls to 25% of porosity for all clay-containing soils; silty loam and loam reach this value at  $-10^\circ$  and  $-5^\circ\text{C}$ ; sand, loamy sand, and sandy loam at  $-1^\circ\text{C}$ . This means organic soils freeze quickest; clay-containing soils freeze later than those without clay.

##### a. Theoretical analysis

###### 1) OVERVIEW

Uncertainty in predicted state variables (first moments) strongly grows with increasing absolute value of the temperature and/or moisture gradient (Figs. 3 and 4). Consequently, uncertainty is higher in soils experiencing huge changes by heating/cooling, and/or infiltration/evapotranspiration than in soils with marginal or no changes (in the diurnal/seasonal course). Above  $0^\circ\text{C}$ , uncertainty is negligibly small for all soils. Below  $0^\circ\text{C}$ , temperature and moisture uncertainty is the greatest (lowest) in the temperature-moisture regime above (below) the freeze-thaw curve where water and ice cannot (can) coexist under these temperature-moisture conditions and consequently (no) phase transitions occur. Since the freeze-thaw curves differ for the various soils, high standard deviations occur at different temperature-moisture regimes for various soils (Fig. 2). Investigation of Eqs. (1) and (2) shows that the freeze-thaw term dominates temperature and moisture uncertainty during phase transition.

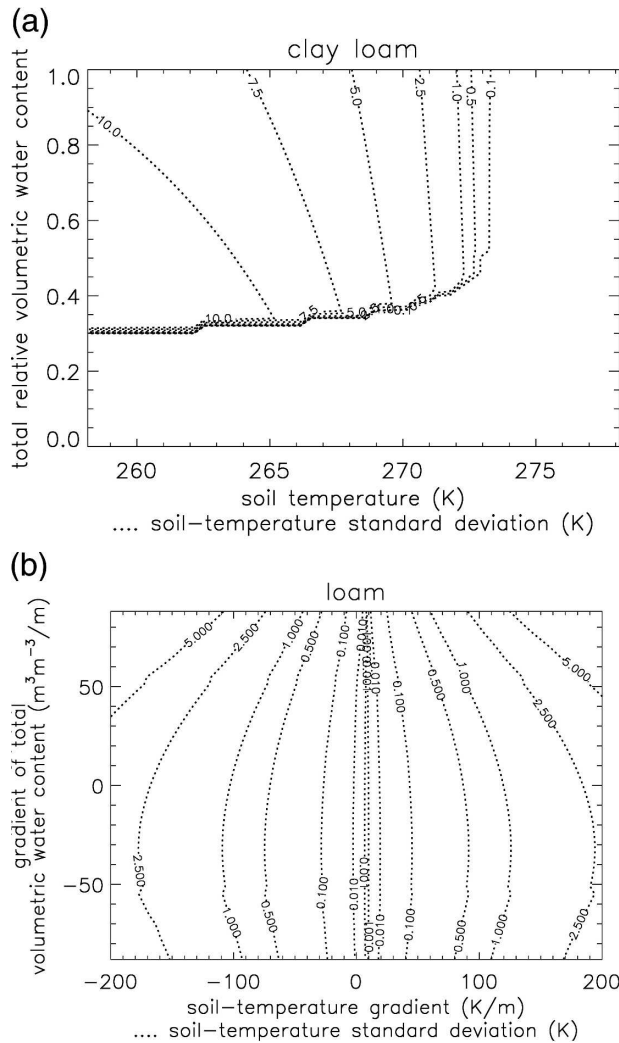


FIG. 3. Soil-temperature uncertainty dependence of (a) soil temperature and volumetric water content (example shown for clay loam) and (b) soil-moisture and -temperature gradient (example shown for loam).

Typically, if predicted fluxes (second moments) approach zero, uncertainty skyrockets. For nonzero fluxes, uncertainty grows with increasing absolute value of the flux. The steepness of the increase depends on soil type; that is, at identical temperature-moisture conditions, soil fluxes and their uncertainties differ for various soils. Generally, relative errors are greater for fluxes than for state variables because the former depend on the gradient of the state variables.

As compared to hydraulic parameters, uncertainty in thermal parameters of dry soil material hardly contributes to temperature and soil-heat-flux uncertainty except above the freeze-thaw curve. Here, contributions by thermal parameters are still smaller than those by hydraulic parameters. The reasons are manifold. The relative errors of the thermal parameters are much

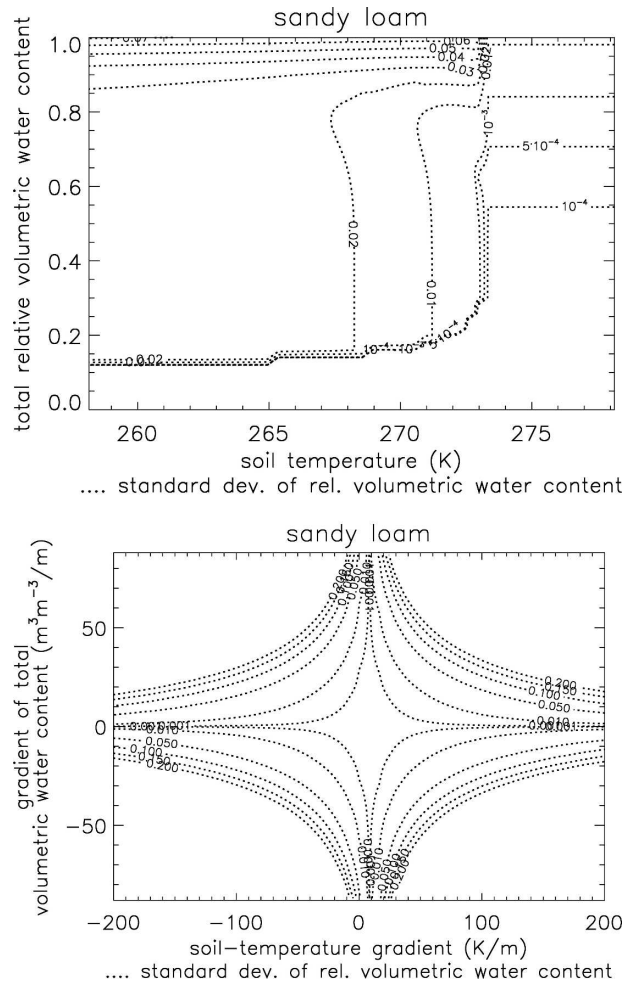


FIG. 4. As in Fig. 3, but for soil moisture. Example shown for sandy loam.

smaller than those of the hydraulic parameters (see Table 1), and they are linear in the terms of Eqs. (1) and (7). On the contrary, the hydraulic parameters occur in nonlinear relations in Eqs. (1)–(6) and Eqs. (8)–(10). These findings suggest that better knowledge of soil hydraulic parameters offers a greater potential for reducing statistical uncertainty in soil-temperature and heat-flux prediction than increasing the current accuracy of soil thermal quantities.

Generally, organic soils bear the greatest uncertainty (Tables 2 and 3); this may however be an artifact, as data for organic soils have been obtained from a wider variety of sources than data for mineral soils. A sensitivity study performed with the standard deviations given by Clapp and Hornberger (1978) provided results similar to those based on Cosby et al.'s (1984) data presented in the following. Therefore, we restrict our discussion to the results obtained with the more recent data.

TABLE 2. Soil parameters found to cause high uncertainty in the indicated predicted soil temperature  $T_s$ , volumetric water content  $\eta$ , soil moisture  $W_s$ , and soil-heat flux  $H_s$ . Uncertainties in density and specific heat capacity of dry soil material contribute negligibly, and saturated hydraulic conductivity contributes less than pore-size distribution index, porosity, or saturated water potential under most soil conditions (therefore not included in this table). Parentheses denote quantities where the indicated parameter is only critical under certain conditions (see text for further details).

Soil type	Porosity	Pore-size distribution index	Saturated water potential
Sand	$\eta, (W_s), H_s$	$T_s, (W_s)$	
Loamy sand		$T_s, (W_s)$	$(T_s)$
Sandy loam	$W_s$	$T_s, \eta, (W_s), H_s$	
Silt loam	$W_s$	$T_s, \eta, (W_s), H_s$	
Loam		$T_s, \eta, (W_s), H_s$	
Sandy clay loam	$W_s$	$T_s, \eta, (W_s), H_s$	
Silty clay loam		$T_s, \eta, (W_s), H_s$	
Clay loam	$W_s$	$T_s, \eta, (W_s), H_s$	
Sandy clay	$W_s$	$T_s, \eta, (W_s), H_s$	
Silty clay		$T_s, \eta, (W_s), H_s$	
Clay		$T_s, \eta, (W_s), H_s$	
Peat soil	$W_s$	$(W_s)$	
Moss soil	$\eta$	$\eta, (W_s)$	$W_s$
Lichen soil	$(W_s)$	$(W_s)$	$\eta$

2) SOIL TEMPERATURE

In all mineral soils, soil-temperature uncertainty remains below 0.5 K for all relative volumetric water-content values at temperatures above 0°C (e.g., Fig. 3). Because of different freeze–thaw curves, the temperature-moisture range of relatively dry supercooled soil

TABLE 3. Soils with on average high (H) and low (L) uncertainty for the soil temperature  $T_s$ , volumetric water content  $\eta$ , soil-heat flux  $H_s$ , soil-moisture flux  $W_s$ , thermal conductivity  $\lambda$ , and hydraulic conductivity  $K_w$ . Uncertainty is judged with respect to the absolute uncertainty for other soils. Note that uncertainty for Eq. (12) is an order of magnitude less than for Eq. (8) even if uncertainty is indicated as H.

Soil type	$T_s$	$\eta$	$H_s$	$W_s$	$\lambda$	$\lambda$	$K_w$
					[Eq. (8)]	[Eq. (12)]	
Sand	L		L	L	H		L
Loamy sand		L	L	L	H		
Sandy loam		L	L		H		
Silt loam					H	L	
Loam					H		
Sandy clay loam					H	L	
Silty clay loam					H	L	H
Clay loam			H		H	L	H
Sandy clay	L	L	H	H	H	L	H
Silty clay			H		H	L	H
Clay		L	H	H	H	L	H
Peat soil	H	H	H	L	H	H	
Moss soil		H	H	L	H	L	
Lichen soil		H	H	L	H	L	L

where soil-temperature uncertainty is low (<0.1 K) is greater for clay-containing soils than other soils. This shift toward relatively wetter conditions goes along with a shift of the maximum standard deviations to wetter conditions.

Above the freeze–thaw curve, sandy clay and sand have the lowest standard deviations (<7.5 K), followed by sandy loam and clay (<10 K); in all other mineral soils, standard deviation exceeds 10 K (e.g., Fig. 3). For organic and mineral soils, uncertainty shows a qualitatively similar pattern. Moss is the organic soil with the lowest (<5 K) soil-temperature prediction uncertainty (Table 3).

For sand, loamy sand, and sandy loam,  $\{T_s, \sigma_b\}$  exceeds the contributions of the other terms to temperature uncertainty by an order of magnitude, on average (Table 2). For all mineral soils,  $\{T_s, \sigma_b\}$  gains importance as the absolute value of the temperature and/or moisture gradient grows. On average,  $\{T_s, \sigma_{\psi_s}\}$  is twice as high as  $\{T_s, \sigma_{\eta_s}\}$  for loamy sand.

3) SOIL MOISTURE

Above the freeze–thaw curve, volumetric water-content uncertainty increases with decreasing temperature until the temperature is reached where only about 25% of the volumetric water at saturation may remain liquid (e.g., Fig. 4). Above a critical value of relative volumetric water content  $\eta/\eta_s$ , which differs with soil type, uncertainty increases with increasing  $\eta/\eta_s$  in the freeze–thaw region. Above 0°C, uncertainty also grows with increasing  $\eta/\eta_s$ . This means that soil-moisture prediction bears more uncertainty in wet than dry soils.

The afore-described nonlinear growth of moisture uncertainty with increasing moisture (e.g., Fig. 4) results from nonlinear growth of water-transfer coefficients with increasing relative volumetric water content (Fig. 5). This means that rain or meltwater can increase moisture uncertainty by more than an order of magnitude, as soil moistens (e.g., Fig. 6).

On average,  $\{\eta, \sigma_b\}$  contributes an order of magnitude more to moisture uncertainty than the other terms for sandy loam, silt loam, loam, sandy clay loam, and moss, and two orders of magnitude more for silty clay loam, silty clay, and clay loam (Table 2). The dominance of  $\{\eta, \sigma_b\}$  grows with increasing absolute value of the temperature and/or moisture gradient at temperatures below 0°C. On average, for sand and moss  $\{\eta, \sigma_{\eta_s}\}$  exceeds the other terms by about an order of magnitude. This means that for the aforementioned soils  $b$ , and for the last-mentioned soils  $\eta_s$ , should be determined with higher accuracy to improve soil-moisture predictions. For lichen,  $\{\eta, \sigma_{\psi_s}\}$  is two orders of magnitude greater than  $\{\eta, \sigma_{k_s}\}$ .

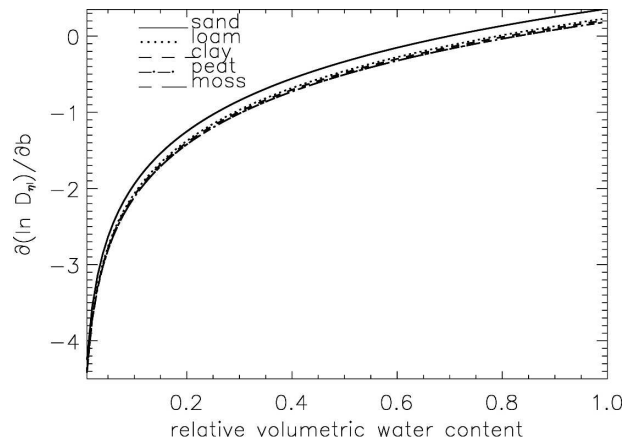


FIG. 5. Uncertainty in water-transfer coefficients. Note the water-transfer coefficient  $D_{\eta_i}$  depends on pore-size distribution index, saturated hydraulic conductivity, saturated water potential, and porosity (cf. Kramm 1995).

#### 4) SOIL-MOISTURE FLUX

Given the same relative volumetric water-content and temperature conditions, the various soils provide different soil-moisture fluxes and hence uncertainty. Soils with high clay fraction allow for the highest (lowest) soil-moisture fluxes at high (low) relative water content  $\eta/\eta_s$  of all soils. Over large temperature-moisture ranges, moisture-flux uncertainty is lower than the flux, and uncertainty grows with increasing absolute flux value. Uncertainty grows with increasing  $\eta/\eta_s$  for all soils (Fig. 7).

At temperatures above  $0^\circ\text{C}$ , soil-moisture fluxes and their uncertainty marginally depend on soil temperature (Fig. 7). Only for  $\eta/\eta_s$  less than 0.15 the influence of the heat-transfer coefficient, and hence temperature, is manifested as a slight slope in the contour lines. Fluxes and their uncertainties are smaller below than above  $0^\circ\text{C}$ , and smallest below the freeze-thaw curve. Thus, predicted soil-moisture fluxes bear more statistical uncertainty during rain, when soils are wet, or non-frozen, than under dry or frozen ground conditions (e.g., Fig. 8).

Obviously, all soils have a range of  $\eta/\eta_s$  and  $T_s$  combinations wherein differences between soil-moisture flux and its uncertainty are maximal; that is, relative errors are minimal. In clay loam, for instance, the lowest relative error exists at soil temperatures below 263 K and relative volumetric water content between 0.3 and 0.5; in loam, below 257 K and at  $\eta/\eta_s$  between 0.2 and 0.4.

On average  $\{W_s, \sigma_{\eta_s}\}$  dominates moisture-flux uncertainty for sand, sandy loam, silt loam, sandy clay loam, clay loam, sandy clay, peat, and lichen, while  $\{W_s, \sigma_{\psi_s}\}$  dominates for moss.

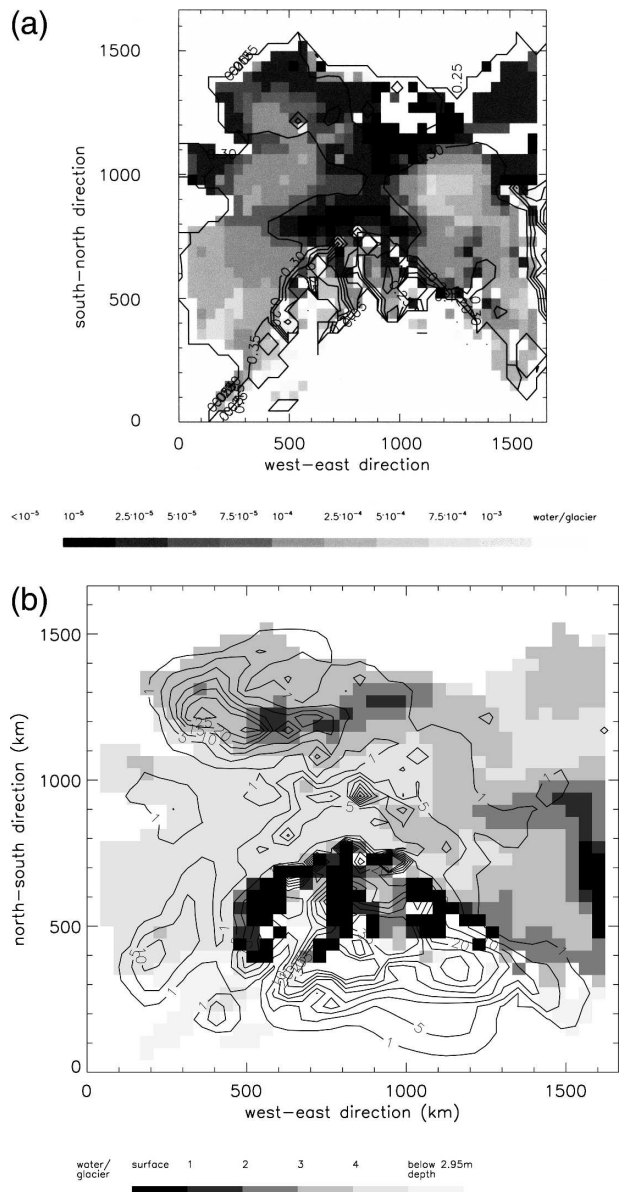


FIG. 6. Horizontal distribution of (a) volumetric water content (contour lines) and its uncertainty (gray shading) in the second soil layer (counted from the surface) after 45 h of simulation ( $\text{m}^3 \text{m}^{-3}$ ), and (b) 84-h-accumulated precipitation (lines) and layer of the freezing line (shaded) at start of simulation.

Examination of the Eq. (2) terms shows that sensitivity of the water-transfer coefficient to uncertainty in pore-size distribution index dominates moisture-flux uncertainty, on average, because the term  $(\partial D_{\eta_i}/\partial b)$  nonlinearly increases with growing relative volumetric water content (Fig. 5). Since most modern soil models are based on the Richards equation we must accept that this uncertainty currently limits soil modeling in general. Therefore, an urgent need exists to determine

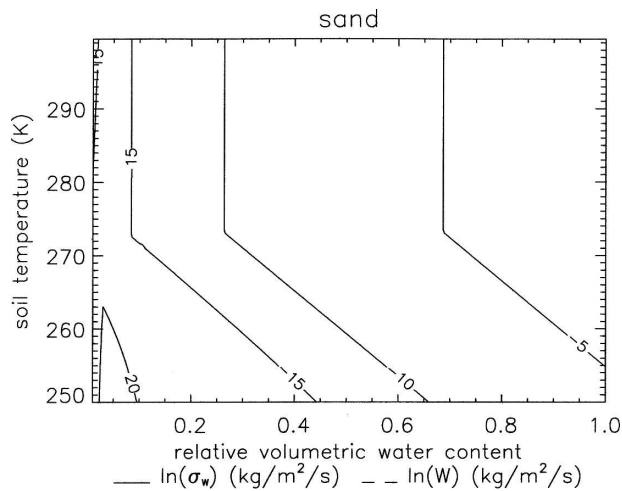


FIG. 7. Relationship between logarithm of soil-moisture fluxes and logarithm of parameter-induced uncertainty in the fluxes at various soil-temperature and relative volumetric water content conditions. A difference in volumetric water content of  $0.05 \text{ m}^3 \text{ m}^{-3}$  over  $0.05 \text{ m}$  was assumed for calculations. Example shown for sand.

more accurate values for  $b$  and develop an improved parameterization for  $D_{\eta l}$ .

### 5) SOIL-HEAT FLUX

At soil temperatures above  $0^\circ\text{C}$ , soil-heat fluxes decrease with diminishing total moisture nearly independent of soil temperature (Fig. 9). However, along the freeze–thaw curve,  $H_s$  increases rapidly for decreasing relative total moisture and first increases, then de-

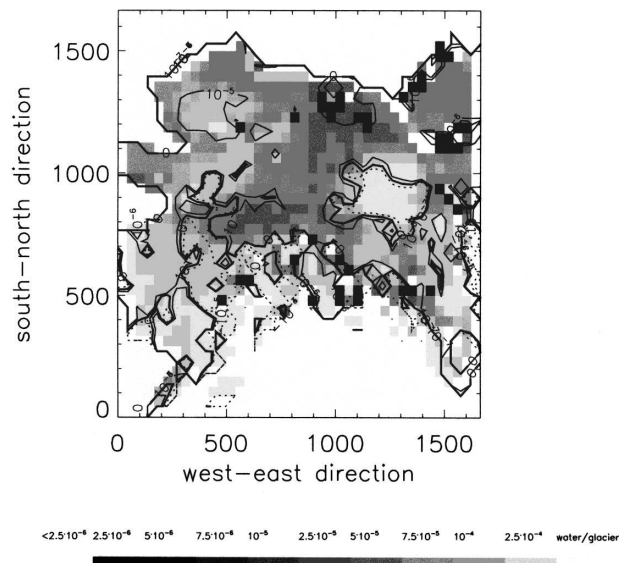


FIG. 8. Horizontal distribution of soil-moisture flux (contour lines) and its uncertainty (gray shading) in the second soil layer (counted from the surface) after 45 h of simulation [ $\text{kg} (\text{m}^2 \text{ s})^{-1}$ ].

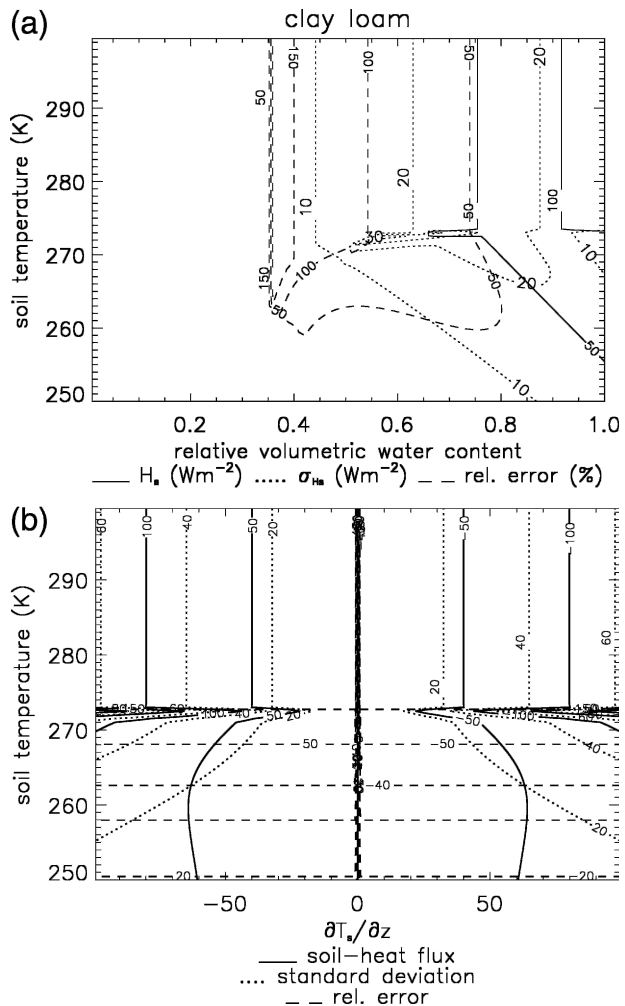


FIG. 9. Soil-heat-flux uncertainty in dependence of (a) soil temperature and total volumetric water content for a gradient of  $0.5 \text{ K}$  over  $0.05 \text{ m}$  (example clay loam), and (b) soil temperature and soil-temperature gradient.

creases as soil temperature lessens. At even lower temperatures,  $H_s$  decreases as temperature or relative total moisture decrease.

For all soils, heat-flux uncertainty is of the same order of magnitude as typical errors in soil-heat flux measurements. Heat-flux uncertainty increases slightly with increasing absolute value of soil-heat flux. The absolute value of soil-heat flux and its relative error decreases with increasing relative volumetric water content, indicating that  $H_s$  is more reliable after rain (e.g., Fig. 10) or in the Tropics than during drought or in deserts.

Uncertainty is greater for great than small absolute values of temperature gradients except if the flux approaches zero (e.g., Fig. 9). At soil temperatures below  $0^\circ\text{C}$ , heat-flux uncertainty exhibits a slight nonlinear decrease with decreasing soil temperature for negative

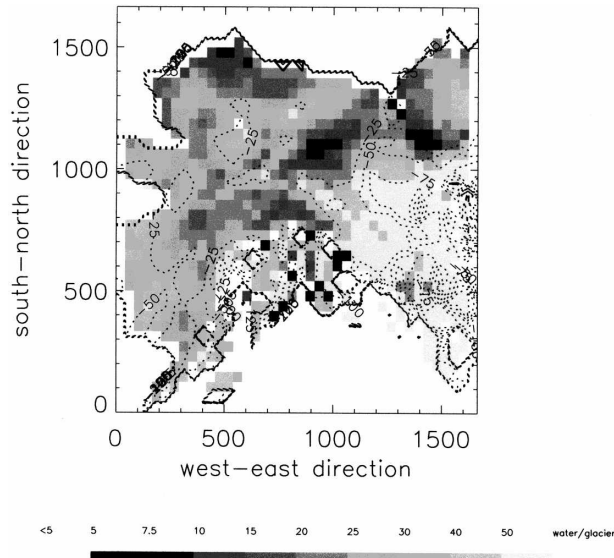


FIG. 10. As in Fig. 8, but for soil-heat flux ( $\text{W m}^{-2}$ ).

and positive temperature gradients ( $\partial T_s/\partial z$ ) and is independent of soil temperature above  $0^\circ\text{C}$ . The steepness of the decrease (increase) depends on soil type. Relative errors are maximal above the freeze-thaw curve. In this temperature-moisture range, uncertainty decreases nonlinearly toward colder and drier soil conditions.

On average, relative error increases in the following order: sand, loamy sand, sandy loam, silty loam, loam, sandy clay loam, silty clay loam, clay loam, sandy clay, silty clay, clay, organic soils (Table 3). For some soil temperature and soil-temperature gradient conditions individual relative errors may exceed 50%.

For silt loam, sandy clay loam, silty clay loam, clay loam, silty clay, and clay,  $\{H_s, \sigma_b\}$  exceed the contributions of other terms to heat-flux uncertainty by one or two orders of magnitude, on average. In sand,  $\{H_s, \sigma_{\eta_s}\}$  dominates heat-flux uncertainty (Table 2).

Since most modern soil models use the soil-heat-diffusion equation for  $H_s$ , individual terms derived for Eq. (1) are analyzed. Excluding the cross effects [i.e.,  $\rho_w L_v D_{\eta_w} (\partial \eta / \partial z) = 0$ ], which is frequently done to increase computational performance, shows that this term does not cause great soil-heat-flux uncertainty. The Dufour effect term leads to the behavior found for dry-warm soil (Fig. 9). The examination also showed that parameterization of thermal conductivity [Eq. (8)] dominates heat-flux uncertainty, on average.

## 6) THERMAL CONDUCTIVITY

Thermal conductivity  $\lambda$  as given by Eq. (8) depends on  $b$ ,  $\psi_s$ , and  $\eta_s$ , and shows nonlinear behavior (Fig. 11).

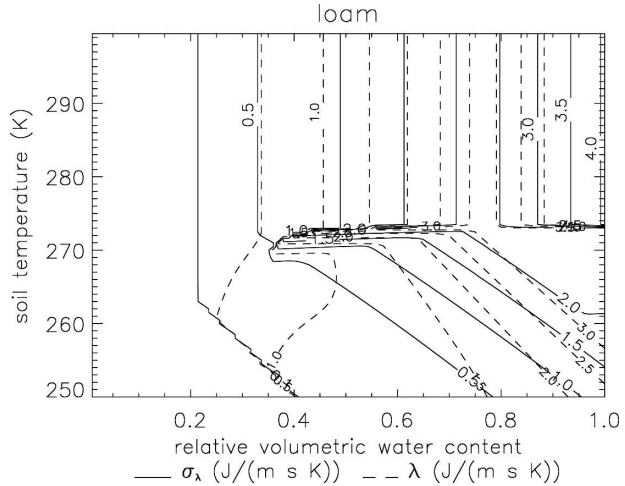


FIG. 11. Relationship between thermal conductivity given by Eq. (8) and its uncertainty at various soil-temperature and relative volumetric water content conditions. Example shown for loam.

For all soils,  $\lambda$  and its uncertainty less strongly decrease with  $\eta/\eta_s$  below  $0^\circ\text{C}$  than above  $0^\circ\text{C}$ , and grow with decreasing soil temperature. This increase is stronger for high than low  $\eta/\eta_s$ . Thermal conductivity and its uncertainty are temperature independent for soils warmer than  $0^\circ\text{C}$ . On average, uncertainty is greatest for loamy sand and least for clay, but still unacceptably great (Table 3). Uncertainty of thermal conductivity is greatest for wet hot soils (e.g., Tropics), and lowest for dry frozen ground (e.g., midlatitudes winter). Note that based on First International Satellite Land Surface Climatology Project (ISLSCP) Field Experiment (FIFE) data, Peters-Lidard et al. (1998) reported under- overestimation of  $\lambda$  for wet/dry periods when Eq. (8) is used.

Despite the huge relative errors of  $\psi_s$  ( $\varepsilon_{\psi_s} > 100\%$ ; cf. Table 1), uncertainty of  $\eta_s$  and  $b$  contribute more strongly to soil-heat-flux standard deviation than does that of  $\psi_s$  (Table 2). Consequently, increasing the accuracy of  $\eta_s$  and  $b$  provides more potential for improving soil modeling than increasing the accuracy of  $\psi_s$ .

We modified Farouki's (1981) approach, commonly used in permafrost modeling, for application in HTSVS,

$$\lambda = \lambda_s^{(1-\eta_s)} \lambda_w^\eta \lambda_{\text{ice}}^{\eta_{\text{ice}}} \lambda_a^{(\eta_s - \eta - \eta_{\text{ice}})}, \quad (12)$$

and determined its parameter-induced statistical uncertainty. The only soil parameters occurring in this parameterization are thermal conductivity of dry soil material,  $\lambda_s$ , and porosity. Thermal conductivity of water  $\lambda_w [=0.57 \text{ W (m K)}^{-1}]$ , ice  $\lambda_{\text{ice}} [=2.31 \text{ W (m K)}^{-1}]$ , and air  $\lambda_a [=0.025 \text{ W (m K)}^{-1}]$  are physical constants.

Although Eq. (12) provides lower thermal conduc-

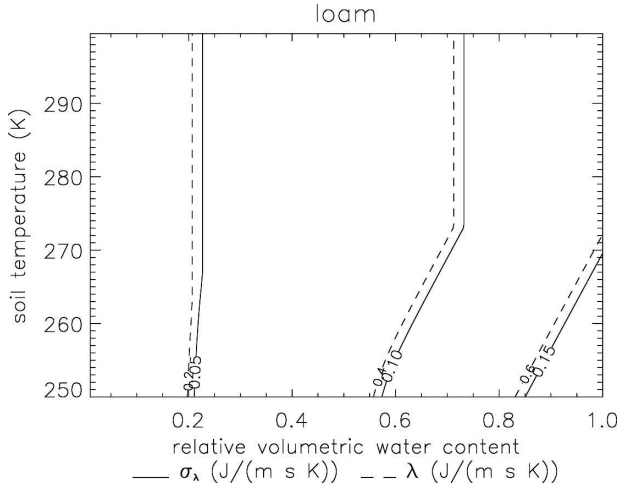


FIG. 12. Like Fig. 11, but for thermal conductivity given by Eq. (12). Example shown for loam.

tivity values than Eq. (8), they fall in the range typically measured in Alaska (V. E. Romanovsky 2004, personal communication). Moreover, parameter-induced uncertainty in thermal conductivity is lower than when using HTSVS' original formulation and behaves less nonlinearly along the freeze–thaw curve (cf. Figs. 11 and 12).

The differences in soil-heat fluxes obtained with the two parameterizations are of the same size as measurement errors. Thus, current measurements do not allow assessing the superiority of one parameterization for thermal conductivity over another. However, the method illustrated here may serve as an objective measure for evaluating model improvement. As the parameter-induced uncertainty decreases when applying Eq. (12), it is suggested this formulation be used in future soil-model applications.

### b. Application

Because moisture and heat fluxes are coupled [see Eqs. (1)–(10)], precipitation can affect thermodynamic state, particularly in the upper soil. Thus, the simulated precipitation distribution is briefly described. For 21 July, MM5 predicts about 30- and 20-mm precipitation in the Alaska and Brooks Ranges, respectively, and heavy showers in western Alaska and the Interior, locally accumulating 7 mm. For 22 (23) July, precipitation up to 7.5 (5) mm is predicted in the Brooks Range and 23 (36) mm in the Alaska Range. In the last 12 h of the simulation, more than 22, 28, and 6 mm are predicted for the Interior, Alaska Range, and Brooks Range, respectively. Traces of precipitation and local showers occur in Yukon Territory and western Alaska.

The soil distribution, climatic, terrain, and soil-

moisture conditions lead to the following picture: Counted from the surface, on the North Slope, frozen ground exists in the third layer and deeper, and in the third or fourth layer in the Interior. In Yukon Territory, Alaska Range, and toward the end of the episode in the Brooks Range, frozen ground locally occurs at the surface. The deepest soil layer holds permafrost everywhere except along the Gulf of Alaska (Fig. 6).

Because statistical uncertainty in thermal conductivity propagates into soil-temperature and heat-flux uncertainty, a simulation was performed using Eq. (12). This simulation provided slightly altered distributions of  $T_s$  and  $H_s$  with, on average, lower uncertainties than those of the simulation discussed in the following. As in HTSVS, soil-temperature and soil-moisture states are coupled;  $W_s$ ,  $\eta$ , and hence their uncertainty changes slightly too. These changes are small compared to the reduced parameter-induced uncertainty found for  $T_s$  and  $H_s$ . Note that slight changes in state variables and fluxes slightly affected precipitation (onset, distribution, amount) due to altered water and energy fluxes to the atmosphere. As no three-dimensional (3D) fields of observed thermal conductivity exist, improvement of MM5–HTSVS with the alternative parameterization can only be evaluated indirectly, if at all, by assessing overall performance in the future.

In the following, soil-heat and water fluxes having a positive (negative) sign are directed toward the atmosphere (soil) and mean a cooling (heating) of the soil.

### 1) OVERVIEW

Typically, uncertainty and the contributions of  $\{\phi, \sigma_{\lambda_i}\}$  decrease with depth (up to more than an order of magnitude) for all fluxes and state variables (e.g., Fig. 13) except at soil conditions above those characterized by the freeze–thaw curve. Here, uncertainty in predicted  $T_s$  and  $\eta$  reaches up to 6.1 K and  $0.19 \text{ m}^3 \text{ m}^{-3}$  when phase transitions occur. Great uncertainty exists in areas experiencing a diurnal freeze–thaw cycle (e.g., Figs. 6 and 14). In deep soil, state variables and fluxes and their uncertainties hardly change with time. Increased reliability at deeper layers results from lower vertical temperature and moisture gradients and temporal changes in the permafrost soils. Note that some studies (e.g., Bastidas et al. 2003; Yang et al. 2005) found different results for soils in other areas; that is, the uncertainty behavior with respect to depth cannot be generalized. When applying inverse estimates of soil properties, for instance, Yang et al. (2005) reported greater errors for their deeper layers for a Tibet field experiment. It has to be examined in the future whether our findings are due to the fact that we assume the same soil type at all depth.

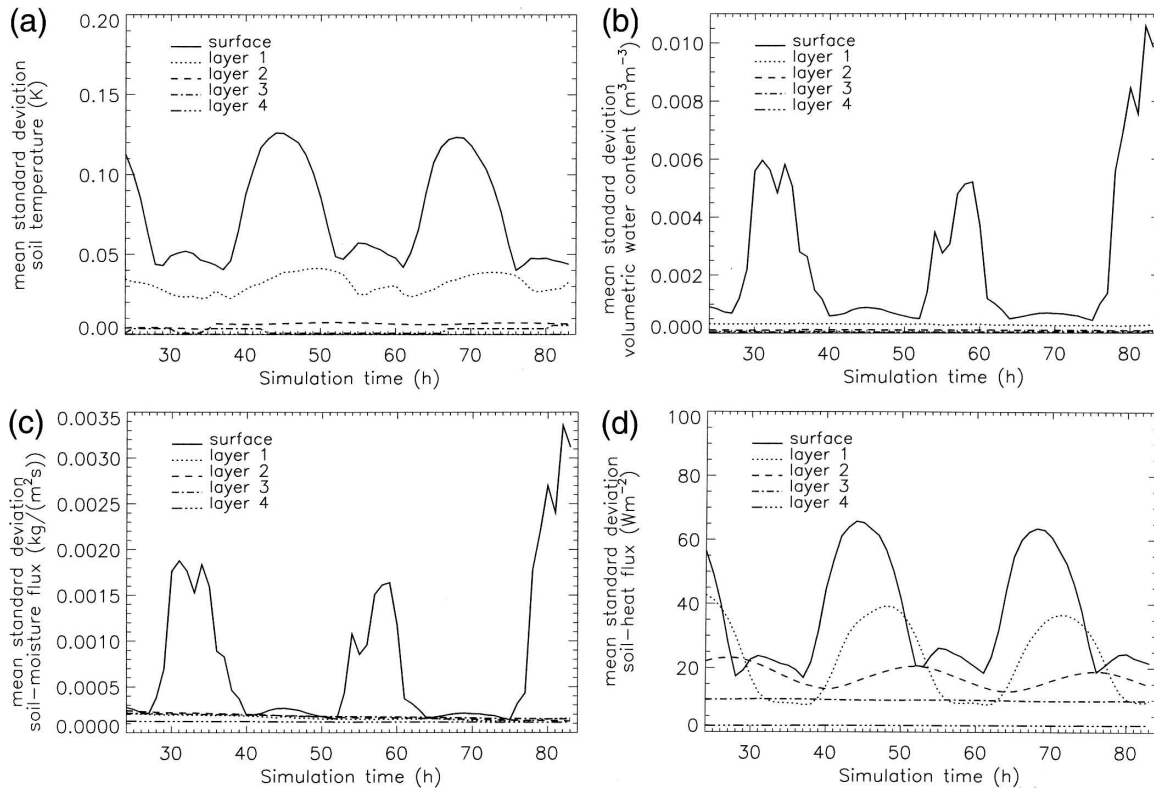


FIG. 13. Temporal evolution of uncertainty in (a) soil temperature, (b) volumetric water content, (c) soil-moisture fluxes, and (d) soil-heat fluxes averaged over all land grid points at various depths. Results shown are after spinup.

In the 3D simulation, the soil-type dependency of the flux–uncertainty relationship is less obvious than in the theoretical analysis because the same flux value and uncertainty can result from other temperature–moisture combinations for different soils. At the surface, moreover, vegetation fraction and type indirectly influence soil fluxes.

Uncertainty of state variables and fluxes shows a diurnal course in the uppermost soil layer, being most evident for  $H_s$  and  $T_s$  (e.g., Fig. 13). For the given soil conditions, uncertainty is usually greater by day than at night. Precipitation strongly disturbs the diurnal cycle, because percolating water increases moisture flux and its induced heat transport can affect phase-transition processes [cf. Eqs. (1) and (2)].

## 2) SOIL TEMPERATURE

At low elevation, daytime soil-surface temperatures reach up to 25°C in cloud-free, and 10°–20°C in cloudy, areas; nighttime values vary between 5° and 15°C. In the upper soil, temperatures are locally below 0°C in the Brooks Range, in Yukon Territory, and the Alaska Range (e.g., Fig. 14). In the deepest layer, temperatures are below 0°C except along the Gulf of Alaska where they may reach 5°C.

From the surface to as deep as the second soil layer beneath the surface, soil-temperature uncertainty shows a maximum around noon (e.g., Fig. 13). A secondary peak occurs around midnight in areas where temperatures are above 0°C by day and lower at night.

In the temperature–moisture range above the freeze–thaw curve (e.g., in the Brooks Range, Alaska Range, Yukon Territory; see Fig. 14) temperature uncertainty is the highest ( $>0.05$  K) and contributions of  $\{T_s, \sigma_{\chi_i}\}$  may reach 1 K. The highest temperature uncertainty exists for sandy loam and loam areas because those soil conditions fall in the range above the freeze–thaw curve. Temperature uncertainty increases when rain moistens the soil. When air temperatures slightly fall during the episode, areas with frozen ground and consequently enhanced temperature uncertainty grow slightly. In deep soil, uncertainty remains less than  $10^{-3}$  K and distribution hardly varies with time.

At the surface,  $\{T_s, \sigma_b\}$ ,  $\{T_s, \sigma_{\eta_s}\}$ , and  $\{T_s, \sigma_{\psi_s}\}$  each contribute about  $5 \times 10^{-3}$  to 0.05 K to temperature uncertainty except at some areas in Yukon Territory, and the Alaska and Brooks Ranges. In the upper soil, areas of clay loam are represented in the distribution of  $\{T_s, \sigma_{\psi_s}\}$  by lower values ( $<5 \times 10^{-3}$  K) than the adjacent soils.

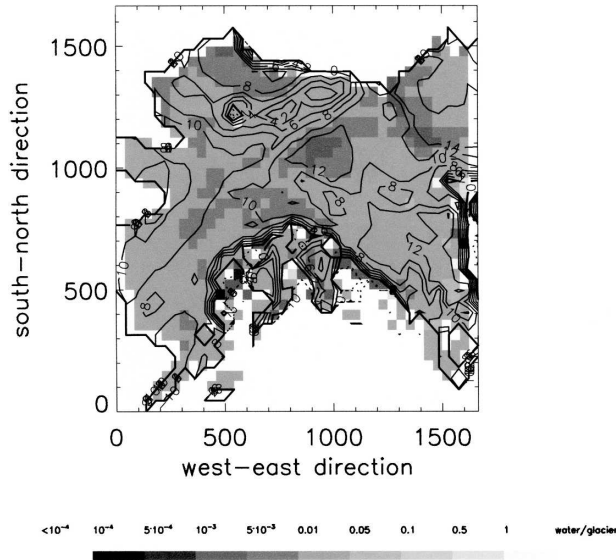


FIG. 14. Horizontal distribution of soil temperature (lines) and its uncertainty (shaded) in second soil layer (counted from the surface) after 45 h of simulation.

### 3) SOIL MOISTURE

In the upper soil layers of Interior and western Alaska and most of Yukon Territory,  $\eta$  ranges from 0.25 to 0.3  $\text{m}^3 \text{m}^{-3}$ , whereas in the Brooks Range, Alaska Range, southern Yukon Territory, and along the Arctic Ocean,  $\eta$  becomes less than 0.1  $\text{m}^3 \text{m}^{-3}$  because of permafrost (e.g., Fig. 6). At the surface, evapotranspiration reduces  $\eta$  slightly by day causing a diurnal cycle in the upper soil (Fig. 13) where  $\eta$  increases when precipitation occurs;  $\eta$  drops right after strong precipitation because of high saturated hydraulic conductivity [cf. Eq. (6)]. Luo et al. (2003) found similar behavior within PILPS. In deep soil, clay loam has low ice content, and  $\eta$  still varies between 0.15 and 0.2  $\text{m}^3 \text{m}^{-3}$ . Along the Gulf of Alaska,  $\eta$  ranges from 0.25 to 0.4  $\text{m}^3 \text{m}^{-3}$ .

Surface-moisture uncertainty remains below  $5 \times 10^{-4} \text{m}^3 \text{m}^{-3}$  except for some locations in Yukon Territory, and for areas of precipitation. The lowest uncertainty exists in the Brooks and Alaska Ranges. In the upper soil (e.g., Fig. 6), moisture uncertainty is two orders of magnitude lower in clay-loam areas ( $<10^{-6} \text{m}^3 \text{m}^{-3}$ ) than in their surroundings ( $<10^{-4} \text{m}^3 \text{m}^{-3}$ ). Surface-moisture uncertainty reaches up to  $1.9 \times 10^{-3} \text{m}^3 \text{m}^{-3}$  during precipitation, on average. Once all water has infiltrated,  $\eta$  and its inherent uncertainty decrease again.

Typically, no changes in response to atmospheric demands (water uptake by roots for transpiration, upward soil-moisture fluxes in response to evaporation) can be

detected in moisture uncertainty beneath the uppermost layer except for clay and clay loam. The higher tolerance of these soil types for coexistence of ice and supercooled water (Fig. 2) explains why atmospheric demands can affect deeper soil layers. Thus, diurnal temperature variations cause fewer changes in partitioning between solid and liquid phases in all clay soils than in other soils.

In loam and sandy loam, maximum relative supercooled water content decreases rapidly as temperatures decrease during our episode. Thus, appreciable uncertainty exists in these areas. In deeper soil, moisture uncertainty remains highest in loam and smallest in clay and clay loam, but relative errors are small. In the deepest soil layer, values are negligible ( $<10^{-8} \text{m}^3 \text{m}^{-3}$ ) in areas of continuous (Yukon Territory, Alaska Range, Brooks Range, North Slope) and discontinuous ( $<10^{-7} \text{m}^3 \text{m}^{-3}$ ; Interior, western Alaska) permafrost.

Of all hydraulic parameters, uncertainty in  $k_s$  contributes the least ( $<10^{-5} \text{m}^3 \text{m}^{-3}$  nearly everywhere) to moisture uncertainty in the upper soil. In the Alaska Range, Brooks Range, parts of Yukon Territory, along the Arctic Ocean, and in clay loam,  $\{\eta, \eta_s\}$  remains negligible in the upper soil. Elsewhere this term amounts to between  $5 \times 10^{-6}$  to  $5 \times 10^{-4}$  and  $5 \times 10^{-5}$  to  $10^{-4} \text{m}^3 \text{m}^{-3}$  in areas without and with precipitation, respectively. In the upper soil of the Alaska Range, Yukon Territory, Interior, and along the Gulf of Alaska,  $\{\eta, \sigma_b\}$  ranges between  $2.5 \times 10^{-5}$  and  $7.5 \times 10^{-5} \text{m}^3 \text{m}^{-3}$ ; it is less elsewhere, and even negligible on the North Slope, in the Brooks Range, and in parts of the Alaska Range. In the upper soil, contributions by  $\{\eta, \sigma_{\psi_s}\}$  stay below  $10^{-4} \text{m}^3 \text{m}^{-3}$  nearly everywhere, and are negligible in the Brooks Range, Alaska Range, parts of Yukon Territory, and in clay loam.

### 4) SOIL-MOISTURE FLUX

By day, upward soil-moisture fluxes [up to  $10^{-4} \text{kg} (\text{m}^2 \text{s})^{-1}$ ] occur almost everywhere at the surface except along the Gulf of Alaska and at some locations in Interior and western Alaska and Yukon Territory. At night, surface soil-moisture fluxes remain positive north of the Arctic Circle because here evapotranspiration still occurs. Here,  $W_s$  penetrates upward all day in the uppermost soil layer to fulfill atmospheric demands (e.g., Fig. 8). Soil-moisture fluxes bear more statistical uncertainty in cloudless than in rain-free cloudy areas, because in the former evapotranspiration is usually higher than in the latter. Moisture-flux uncertainty is an order of magnitude greater during and just after precipitation than before precipitation onset. Precipitation impact on moisture-flux uncertainty decreases with depth and after precipitation, as  $W_s$  decreases. In the

second soil layer beneath the surface, soil-moisture fluxes are less than  $10^{-4} \text{ kg (m}^2 \text{ s)}^{-1}$  (e.g., Fig. 8). Here, they hardly show a diurnal cycle, but still respond slightly to precipitation. In deeper soil layers,  $W_s$  becomes negligible in permafrost and small in unfrozen soil.

At the surface, moisture-flux uncertainty remains below  $3.4 \times 10^{-3} \text{ kg (m}^2 \text{ s)}^{-1}$ , on average (Fig. 13), with the greatest uncertainty for loamy sand, and the smallest for clay loam and clay [ $<10^{-4} \text{ kg (m}^2 \text{ s)}^{-1}$ ]. Note that the former areas received precipitation locally, while the latter did not.

Close beneath the surface (e.g., Fig. 8), clay loam areas are represented in the distribution of moisture-flux uncertainty by lower values [ $<5 \times 10^{-6} \text{ kg (m}^2 \text{ s)}^{-1}$ ] as compared to their surroundings [ $2.5 \times 10^{-5}$ – $5 \times 10^{-5} \text{ kg (m}^2 \text{ s)}^{-1}$ ]. In the third layer beneath the surface, sandy loam areas are indicated by higher uncertainty values [up to  $10^{-4} \text{ kg (m}^2 \text{ s)}^{-1}$ ] than adjacent soils [ $<10^{-5} \text{ kg (m}^2 \text{ s)}^{-1}$ ]. At deep layers, moisture-flux uncertainty is less than  $10^{-7} \text{ kg (m}^2 \text{ s)}^{-1}$  in permafrost and less than  $10^{-5} \text{ kg (m}^2 \text{ s)}^{-1}$  elsewhere.

Along the Gulf of Alaska and in Interior and western Alaska,  $\{W_s, \sigma_b\}$  ranges from  $5 \times 10^{-6}$  to  $10^{-5} \text{ kg (m}^2 \text{ s)}^{-1}$ . In permafrost, this term contributes negligibly. Areas of sandy loam are clearly indicated in the distribution of  $\{W_s, \sigma_{\psi_s}\}$  by values lower [ $<2.5 \times 10^{-5} \text{ kg (m}^2 \text{ s)}^{-1}$ ] than those in the environment [ $2.5 \times 10^{-5}$ – $5 \times 10^{-5} \text{ kg (m}^2 \text{ s)}^{-1}$ ]. The same is true for clay loam in deeper soil [ $<10^{-7} \text{ kg (m}^2 \text{ s)}^{-1}$ ]. Uncertainty in  $k_s$  contributes less to moisture-flux uncertainty than all other parameters. In deep soil, clay loam is clearly represented in the  $\{W_s, \sigma_{k_s}\}$  distribution by smaller values [ $<10^{-7} \text{ kg (m}^2 \text{ s)}^{-1}$ ] compared to adjacent soils.

### 5) SOIL-HEAT FLUX

During the episode, soils cool in Interior and western Alaska, in most of Yukon Territory, and in the western North Slope at night. Daytime soil heating is greatest in cloud-free areas, locally at the surface as high as  $150 \text{ W m}^{-2}$  (Yukon Territory). In cloudy areas, heating ranges from 25 to  $50 \text{ W m}^{-2}$ . At night,  $H_s$  varies between  $-25$  and  $50 \text{ W m}^{-2}$ . In some areas,  $H_s$  does not change direction in the diurnal course. Soil-heat fluxes decrease with distance from the surface in the upper soil, but still heat the soil during the day. At deeper layers, of course,  $H_s$  hardly varies with time.

By day, heat-flux uncertainty reaches up to  $50 \text{ W m}^{-2}$  in the Brooks and Alaska Ranges and in cloud-free areas in Yukon Territory, while it remains less than  $30 \text{ W m}^{-2}$  elsewhere (e.g., Fig. 10). At night, uncertainty reduces to less than  $10 \text{ W m}^{-2}$  except for cloud-free areas in western Alaska and southern Yukon Territory

where it remains below  $50 \text{ W m}^{-2}$ . The lowest heat-flux uncertainty exists in permafrost (e.g., Brooks Range, Alaska Range, locally in Yukon Territory). At deeper layers, uncertainty typically reduces to  $5$  ( $20$ )  $\text{W m}^{-2}$  in areas with (without) permafrost.

At the surface and in the upper soil, heat-flux uncertainty shows a maximum around noon (Fig. 13). If  $H_s$  changes direction, uncertainty shows a secondary peak at midnight. Since at this time of year absolute soil-heat-flux values are greater by day than at night, uncertainty of downward soil-heat fluxes exceeds that of upward fluxes. In the third layer, diurnal amplitude still reaches up to  $10 \text{ W m}^{-2}$ , on average.

At soil conditions above those represented by the freeze–thaw curve,  $\{H_s, \sigma_{\psi_s}\}$ ,  $\{H_s, \sigma_{\eta_s}\}$ , and  $\{H_s, \sigma_b\}$  each typically exceed  $20 \text{ W m}^{-2}$ . In deep soil,  $\{H_s, \sigma_{\psi_s}\}$  usually remains less than  $2 \text{ W m}^{-2}$ . In permafrost,  $\{H_s, \sigma_{\psi_s}\}$ ,  $\{H_s, \sigma_{\eta_s}\}$ , and  $\{H_s, \sigma_b\}$  stay below  $0.5 \text{ W m}^{-2}$ .

## 5. Conclusions

We introduced GEP principles to examine model uncertainty in predicted values of  $\eta$ ,  $T_s$ ,  $W_s$ , and  $H_s$  caused by statistical uncertainty of empirical soil parameters occurring in the governing equations of the soil physical processes. This method allows examining the relative importance of these parameters in producing forecast uncertainty at various forecast lead ends. Close beneath the surface, uncertainty undergoes a diurnal course. At most soil temperature-moisture conditions, a quasi-linear relationship exists between the absolute values of  $W_s$  and  $H_s$  and their respective uncertainty; that is, relative predictability is about as good by day as at night.

When phase transitions occur, the freeze–thaw term causes great uncertainty in  $\eta$  and  $T_s$  when compared to the quantities themselves. This explains the great uncertainty throughout the simulation at temperature-moisture conditions above the freeze–thaw curve. Thus, we may conclude that predictions of  $\eta$  and  $T_s$  are least reliable in the active layer close to the freezing line and in moist soils in midlatitude winter as temperature falls.

Our analysis gave evidence that uncertainty in thermal conductivity dominates heat-flux uncertainty. Introducing Farouki's (1981) formulation of thermal conductivity in HTSVS reduced uncertainty in predicted values of  $H_s$  and  $T_s$  especially above the freeze–thaw curve. These findings underline that GEP principles are indispensable for analysis of parameterized soil processes. As documented in Tables 2 and 3, our analysis also identified predictions for soils with high clay fraction as especially uncertain.

Pore-size distribution index was identified as the most critical parameter. Its uncertainty especially domi-

nates uncertainty in  $W_s$  because it causes high relative errors in  $K_w$ . If uncertainty were judged according to the parameters' relative errors,  $k_s$  followed by  $b$  would be classified as the parameters for which higher accuracy would be desirable. Uncertainty in thermal parameters generally contributes less to soil-temperature uncertainty than uncertainty in hydraulic parameters. Even for  $H_s$ , increased accuracy of hydraulic parameters will reduce uncertainty because parameterization of thermal conductivity depends on hydraulic parameters. Since increasing the accuracy of hydraulic parameters offers a greater potential for improvement of soil modeling than doing so for thermal parameters, efforts should focus on achieving the former.

Since GEP showed itself able to identify critical parameters and (parts of) parameterizations, results of GEP analysis could form a basis for prioritizing which parameters to determine with higher accuracy and for intercomparisons of soil models aimed at improving soil modeling.

*Acknowledgments.* We thank the reviewers for helpful discussion and fruitful comments, C. O'Connor for editing, and BMBF and NSF for financial support under contract 07ATF30, ATM-0232198, and OPP-0327664.

#### REFERENCES

- Avissar, R., and R. A. Pielke, 1989: A parameterization of heterogeneous land surface for atmospheric numerical models and its impact on regional meteorology. *Mon. Wea. Rev.*, **117**, 2113–2136.
- Bastidas, L. A., H. V. Gupta, and S. Sorooshian, 2003: Parameter, structure and performance evaluation for land surface models. *Advances in the Calibration of Watershed Models*, *Geophys. Monogr.*, No. 6, Amer. Geophys. Union, 229–238.
- Calder, I. R., R. A. Hall, H. G. Bastable, H. M. Gunston, O. Shela, A. Chirwa, and R. Kafundu, 1995: The impact of land use changes on water resources in sub-Saharan Africa: A modelling study of Lake Malawi. *J. Hydrol.*, **170**, 123–136.
- Calhoun, F. G., N. E. Smeck, B. L. Slater, J. M. Bigham, and G. F. Hall, 2001: Predicting bulk density of Ohio soils from morphology, genetic principles, and laboratory characterization data. *Soil Sci. Soc. Amer. J.*, **65**, 811–819.
- Callies, U., A. Rhodin, and D. P. Eppel, 1998: A case study on variational soil moisture analysis from atmospheric observations. *J. Hydrol.*, **212–213**, 95–108.
- Carey, S. K., and M. Woo, 1999: Hydrology of two slopes in subarctic Yukon, Canada. *Hydrol. Processes*, **13**, 2549–2562.
- Chen, F., and J. Dudhia, 2001: Coupling an advanced land surface hydrology model with the Penn State/NCAR MM5 modeling system. Part I: Model implementation and sensitivity. *Mon. Wea. Rev.*, **129**, 569–585.
- Clapp, R. B., and G. M. Hornberger, 1978: Empirical equations for some soil hydraulic properties. *Water Resour. Res.*, **14**, 601–604.
- Cosby, B. J., G. M. Hornberger, R. B. Clapp, and T. R. Ginn, 1984: A statistical exploration of the relationships of soil moisture characteristics to the physical properties of soils. *Water Resour. Res.*, **20**, 682–690.
- Cuenca, R. H., M. Ek, and L. Mahrt, 1996: Impact of soil water property parameterization on atmospheric boundary layer simulation. *J. Geophys. Res.*, **101D**, 7269–7277.
- de Groot, S. R., 1951: *Thermodynamics of Irreversible Processes*. Interscience, 242 pp.
- de Vries, D. A., 1958: Simultaneous transfer of heat and moisture in porous media. *Eos, Trans. Amer. Geophys. Union*, **39**, 909–916.
- Douville, H., and F. Chauvin, 2000: Relevance of soil moisture for seasonal climate predictions: A preliminary study. *Climate Dyn.*, **16**, 719–736.
- Dudhia, J., 1993: A nonhydrostatic version of the Penn State–NCAR Mesoscale Model: Validation tests and simulation of an Atlantic cyclone and cold front. *Mon. Wea. Rev.*, **121**, 1493–1513.
- Farouki, O., 1981: *Thermal Properties of Soils*. *CRREL Monogr.*, No. 81-1, U.S. Army Cold Regions Research and Engineering Laboratories, 136 pp.
- Flerchinger, G. N., and K. E. Saxton, 1989: Simultaneous heat and water model of a freezing snow–residue–soil system. I. Theory and development. *Trans. ASAE*, **32**, 565–571.
- Gao, X., S. Sorooshian, and H. V. Gupta, 1996: Sensitivity analysis of the Biosphere–Atmosphere Transfer Scheme. *J. Geophys. Res.*, **101D**, 7279–7289.
- Grell, G., Y.-H. Kuo, and R. J. Pasch, 1991: Semi-prognostic tests of cumulus parameterization schemes in the middle latitudes. *Mon. Wea. Rev.*, **119**, 5–31.
- , J. Dudhia, and D. Stauffer, 1994: A description of the fifth-generation Penn State/NCAR Mesoscale Model (MM5). *NCAR/TN-398+STR*, 122 pp.
- Grunwald, S., D. J. Rooney, K. McSweeney, and B. Lowery, 2001: Development of pedotransfer functions for a profile cone penetrometer. *Geoderma*, **100**, 25–47.
- Gutman, G., and A. Ignatov, 1998: The derivation of green vegetation from NOAA/AVHRR data for use in numerical weather prediction models. *Int. J. Remote Sens.*, **19**, 1533–1543.
- Henderson-Sellers, 1993: A factorial assessment of the sensitivity of the BATS land-surface parameterization. *J. Climate*, **6**, 227–247.
- Hong, S.-Y., and H.-L. Pan, 1996: Nonlocal boundary layer vertical diffusion in a medium-range forecast model. *Mon. Wea. Rev.*, **124**, 2322–2339.
- Kramm, G., 1995: *Zum Austausch von Ozon und reaktiven Stickstoffverbindungen zwischen Atmosphäre und Biosphäre*. Marau-Verlag, 268 pp.
- , R. Dlugi, T. Foken, N. Mölders, H. Müller, and K. T. Paw U, 1994: On the determination of the sublayer Stanton numbers of heat and matter for different types of surfaces. *The Proceedings of the EUROTRAC Symposium '94*, P. Borrell, P. M. Borrell, and W. Seiler, Eds., SPB Academic, 644–648.
- , N. Beier, T. Foken, H. Müller, P. Schröder, and W. Seiler, 1996: A SVAT scheme for NO, NO<sub>2</sub>, and O<sub>3</sub>—Model description. *Meteor. Atmos. Phys.*, **61**, 89–106.
- Laurén, A., and J. Heiskannen, 1997: Physical properties of the moor layer in a Scots pine stand. I. Hydraulic conductivity. *Can. J. Soil Sci.*, **77**, 627–634.
- Lohmann, D., and Coauthors, 1998: The Project for Intercomparison of Land Surface Parameterization Schemes Phase (PILPS) phase 2(c) Red–Arkansas river basin experiment:

3. Spatial and temporal analysis of water fluxes. *Global Planet. Change*, **19**, 161–179.
- Luo, L., and Coauthors, 2003: Effects of frozen soil on soil temperature, spring infiltration, and runoff: Results from the PILPS2(d) experiment at Valdai, Russia. *J. Hydrometeorol.*, **4**, 334–351.
- McCumber, M. C., and R. A. Pielke, 1981: Simulation of the effects of surface fluxes of heat and moisture in a mesoscale model. I. Soil-layer. *J. Geophys. Res.*, **86**, 9929–9938.
- Miller, D. A., and R. A. White, 1998: A conterminous United States multilayer soil characteristics dataset for regional climate and hydrological modeling. *Earth Interactions*, **2**. [Available online at <http://EarthInteractions.org>.]
- Mölders, N., 2001: On the uncertainty in mesoscale modeling caused by surface parameters. *Meteor. Atmos. Phys.*, **76**, 119–141.
- , and J. E. Walsh, 2004: Atmospheric response to soil-frost and snow in Alaska in March. *Theor. Appl. Climatol.*, **77**, 77–105.
- , A. Raabe, and G. Tetzlaff, 1996: A comparison of two strategies on land surface heterogeneity used in a mesoscale  $\beta$  meteorological model. *Tellus*, **48A**, 733–749.
- , U. Strasser, K. Schneider, W. Mauser, and A. Raabe, 1997: A sensitivity study on the initialization of surface characteristics in meso- $\beta/\gamma$ -modeling using digitized vs. satellite derived landuse data. *Contrib. Atmos. Phys.*, **70**, 173–187.
- , U. Haferkorn, J. Döring, and G. Kramm, 2003a: Long-term numerical investigations on the water budget quantities predicted by the hydro-thermodynamic soil vegetation scheme (HTSVS)—Part I: Description of the model and impact of long-wave radiation, roots, snow, and soil frost. *Meteor. Atmos. Phys.*, **84**, 115–135.
- , —, —, and —, 2003b: Long-term numerical investigations on the water budget quantities predicted by the hydro-thermodynamic soil vegetation scheme (HTSVS)—Part II: Evaluation, sensitivity, and uncertainty. *Meteor. Atmos. Phys.*, **84**, 137–156.
- Montaldo, N., and J. D. Albertson, 2001: On the use of the force-restore SVAT model formulation for stratified soils. *J. Hydrometeorol.*, **2**, 571–578.
- Niu, G.-Y., and Z.-L. Yang, 2004: The effects of canopy processes on snow surface energy and mass balances. *J. Geophys. Res.*, **109**, D23111, doi:10.1029/2004JD004884.
- Peters-Lidard, C. D., E. Blackburn, X. Liang, and E. F. Wood, 1998: The effect of soil thermal conductivity parameterization on surface energy fluxes and temperatures. *J. Atmos. Sci.*, **55**, 1209–1224.
- Philip, J. R., and D. A. de Vries, 1957: Moisture in porous materials under temperature gradients. *Eos, Trans. Amer. Geophys. Union*, **18**, 222–232.
- Raymond, D., and K. Emanuel, 1993: The Kuo cumulus parameterization. *The Representation of Cumulus Convection in Numerical Models*, Meteor. Monogr., No. 46, Amer. Meteor. Soc., 145–151.
- Reichle, R. H., D. B. McLaughlin, and D. Entekhabi, 2001: Variational data assimilation of microwave radiobrightness observations for land surface hydrology applications. *IEEE Trans. Geosci. Remote Sens.*, **39**, 1708–1718.
- Reisner, J., R. M. Rasmussen, and R. T. Bruintjes, 1998: Explicit forecasting of supercooled liquid water in winter storms using the MM5 mesoscale model. *Quart. J. Roy. Meteor. Soc.*, **124B**, 1071–1107.
- Robock, A., K. Y. Vinnikov, C. A. Schlosser, N. A. Speranskaya, and Y. Xue, 1995: Use of midlatitude soil moisture and meteorological observations to validate soil moisture simulations with biosphere and bucket models. *J. Climate*, **8**, 15–35.
- Schlotzhauer, S. M., and J. S. Price, 1999: Soil water flow dynamics in a managed cutover peat field, Quebec: Field and laboratory investigations. *Water Resour. Res.*, **35**, 3675–3683.
- Shao, Y., and A. Henderson-Sellers, 1996: Modeling soil moisture: A project for intercomparison of land surface parameterization schemes phase 2 (b). *J. Geophys. Res.*, **101D**, 7227–7250.
- , and P. Irannejad, 1999: On the choice of soil hydraulic models in land-surface schemes. *Bound.-Layer Meteorol.*, **90**, 83–115.
- Sievers, U., R. Forkel, M. F. Wilson, A. Henderson-Sellers, R. E. Dickinson, and P. J. Kennedy, 1987: Sensitivity of the Biosphere–Atmosphere Transfer Scheme (BATS) to the inclusion of variable soil characteristics. *J. Climate Appl. Meteorol.*, **26**, 341–362.
- Slater, A. G., A. J. Pitman, and C. E. Desborough, 1998: Simulation of freeze-thaw cycles in general circulation land surface scheme. *J. Geophys. Res.*, **103D**, 11 303–11 312.
- van den Hurk, J. J. M., W. G. M. Bastiaanssen, H. Pelgrum, and E. van Meijgaard, 1997: A new methodology for assimilation of initial soil moisture fields in weather prediction models using Meteosat and NOAA data. *J. Appl. Meteorol.*, **36**, 1271–1283.
- Verseghy, D. L., 1991: CLASS—A Canadian land surface scheme for GCMs. 1. Soil model. *Int. J. Climatol.*, **11**, 111–133.
- Viterbo, P., and A. Beljaars, 1995: An improved land surface parameterization scheme in the ECMWF model and its validation. *J. Climate*, **8**, 2716–2748.
- , —, J.-F. Mahouf, and J. Teixeira, 1999: The representation of soil moisture freezing and its impact on the stable boundary layer. *Quart. J. Roy. Meteor. Soc.*, **125**, 2401–2447.
- Wang, W., and A. Kumar, 1998: A GCM assessment of atmospheric seasonal predictability associated with soil moisture anomalies over North America. *J. Geophys. Res.*, **103**, 28 637–28 646.
- Warrach, K., H.-T. Mengelkamp, and E. Raschke, 2001: Treatment of frozen soil and snow cover in the land surface model SEWAB. *Theor. Appl. Climatol.*, **69**, 23–37.
- Wetzel, P. J., and A. Boone, 1995: A parameterization for land–cloud–atmosphere exchange (PLACE): Documentation and testing of a detailed process model of the partly cloudy boundary layer over heterogeneous land. *J. Climate*, **8**, 1810–1837.
- Yang, K., T. Koike, B. Ye, and L. Bastidas, 2005: Inverse analysis of the role of soil vertical heterogeneity in controlling surface soil state and energy partition. *J. Geophys. Res.*, **110**, D08101, doi:10.1029/2004JD005500.
- Yang, Z.-L., R. E. Dickinson, A. Henderson-Sellers, and A. J. Pitman, 1995: Preliminary study of spin-up processes in land surface models with the first stage data of Project for Intercomparison of Land Surface Parameterization Schemes Phase 1(a). *J. Geophys. Res.*, **100D**, 16 553–16 578.
- , —, A. Robock, and K. Y. Vinnikov, 1997: Validation of the snow submodel of the biosphere–atmosphere transfer scheme with Russian snow cover and meteorological observation data. *J. Climate*, **10**, 353–373.

Copyright of *Journal of Hydrometeorology* is the property of *American Meteorological Society* and its content may not be copied or emailed to multiple sites or posted to a listserv without the copyright holder's express written permission. However, users may print, download, or email articles for individual use.